Open access • Posted Content • DOI:10.1101/2021.09.27.461948

Viral replication in human macrophages enhances an inflammatory cascade and interferon driven chronic COVID-19 in humanized mice. — Source link

Esen Sefik, Rihao Qu, Eleanna Kaffe, Jun Zhao ...+13 more authors

Institutions: Yale University, Rockefeller University, Boston Children's Hospital

Published on: 27 Sep 2021 - bioRxiv (Cold Spring Harbor Laboratory)

Topics: Viral replication, Interferon, Virus, Macrophage and RNA

Viral replication in human macrophages enhances an inflammatory cascade and interferon driven chronic COVID-19 in humanized mice.

Esen Sefik[1], Rihao Qu[1,2], Eleanna Kaffe[1] Jun Zhao[1,2], Caroline Junqueira[3,4,5], Haris Mirza[1], Ricky Brewer[1], Ailin Han[1], Holly Steach[1], Benjamin Israelow[1], Y. Grace Chen[1], Stephanie Halene[6], Akiko Iwasaki[1,9], Eric Meffre[1], Michel Nussenzweig[7], Judy Lieberman[3,4], Craig B. Wilen[1,8,] Yuval Kluger[3], Richard A. Flavell[1,9]

Author information:

1. Department of Immunobiology, Yale University School of Medicine, New Haven, CT, USA.
2. Department of Pathology, Yale University School of Medicine, New Haven, CT, USA.
3. Program in Cellular and Molecular Medicine, Boston Children's Hospital, Boston, MA, USA.
4. Department of Pediatrics, Harvard Medical School, Boston, MA, USA.
5. Instituto René Rachou, Fundação Oswaldo Cruz, Belo Horizonte, Minas Gerais, Brazil.
6. Section of Hematology, Yale Cancer Center and Department of Internal Medicine, Yale University School of Medicine, New Haven, CT.
7. Laboratory of Molecular Immunology, The Rockefeller University, New York, NY, USA.
8. Department of Laboratory Medicine, Yale University School of Medicine, New Haven, CT, USA.
9. Howard Hughes Medical Institute, Yale University School of Medicine, New Haven, CT, USA.

Abstract:

Chronic COVID-19 is characterized by persistent viral RNA and sustained interferon (IFN) response which is recapitulated and required for pathology in SARS-CoV-2 infected MISTRG6-hACE2 humanized mice. As in the human disease, monocytes, and macrophages in SARS-CoV-2 infected MISTRG6-hACE2 are central to disease pathology. Here, we describe SARS-CoV-2 uptake in tissue resident human macrophages that is enhanced by virus specific antibodies. SARS-CoV-2 replicates in these human macrophages as evidenced by detection of double-stranded RNA, subgenomic viral RNA and expression of a virally encoded fluorescent reporter gene; and it is inhibited by Remdesivir, an inhibitor of viral replication. Although early IFN deficiency leads to enhanced disease, blocking either viral replication with Remdesivir or the downstream IFN stimulated cascade by injecting anti-IFNAR2 *in vivo* in the chronic stages

of disease attenuates many aspects of the overactive immune-inflammatory response, especially the inflammatory macrophage response, and most consequentially, the chronic disease itself.

Introduction:

SARS-CoV-2 infection initiates with acute viral infection which resolves in most patients but becomes chronic in about 10-20%[1,2]. Two hallmarks of COVID-19 in severely sick patients and Post-COVID syndrome (PCS) are a sustained interferon (IFN) response and persistent viral RNA which can be detected for months even after resolution of the acute symptoms[3-11]. This chronicity is recapitulated in SARS-CoV-2 infected MISTRG6-hACE2 humanized mice by persistent viral RNA and sustained type I IFN response in lungs up to at least one month after viral inoculation by which time viral titers are detectable but significantly reduced (manuscript in revision)[12]. As in the human disease, monocytes, and macrophages in SARS-CoV-2 infected MISTRG6-hACE2 are central to disease pathology and the main source of proinflammatory cytokines interleukin (IL)-1β, IL-18, TNF-α and IL-6 in infected lungs. Of these cytokines elevated in COVID-19 patients, IL-1β, IL-18 and IL-6 also correlated with disease severity[4-10]. Additional studies are required to fully evaluate the role of these cytokines and the implications of persistent viral RNA, and the IFN response in severe COVID-19 and PCS. The ability of the MISTRG6-hACE2 model to recapitulate key aspects of COVID-19 has enabled us to both learn fundamental mechanisms of disease progression and test possible therapeutics to target these disease mechanisms. Here, we characterized the role of viral RNA in the hyperinflammatory macrophage response *in vivo* and showed that persistent viral RNA production and sustained IFN response is required for pathogenesis in SARS-CoV-2 infected MISTRG6-hACE2. We further show that tissue resident human macrophages take up SARS-CoV-2. Replicating SARS-CoV-2 in these human macrophages initiates an inflammatory cascade that endows infected macrophages with a unique transcriptome and contributes to the downstream type I IFN response. Blocking either viral replication or the downstream IFN response *in vivo* during the chronic phase of the disease attenuates many aspects of the overactive immune-inflammatory response, especially the inflammatory macrophage response, and most consequentially, the disease itself.

Results:

Targeting viral replication and downstream interferon signaling ameliorates chronic COVID-19.

In the MISTRG6 model of COVID-19, SARS-CoV-2 virus peaks at four days post infection (4dpi) and then subsides to levels 1000-fold lower which persist for weeks[12]. Similar to infected humans[3], viral RNA persists at high levels for several weeks. To test whether a viral RNA-dependent type I IFN response was a driver of chronic disease, we treated SARS-CoV-2 infected MISTRG6-hACE2 mice with Remdesivir, anti-IFNAR2 antibody or combination of the two starting 7dpi, by which time viral titers are already significantly reduced (Fig. 1A)[12]. As Remdesivir inhibits viral RNA dependent RNA polymerase (RdRp)[13] while anti-IFNAR2 targets the IFN-dependent cascade downstream of infection, we hypothesized that targeting these two elements which act sequentially would attenuate the hyperactive immune/inflammatory response and resolve immunopathology. As a control, we also treated mice with dexamethasone, one of the few treatments that significantly reduced hospitalization and mortality in the clinic[14]. Dexamethasone in our model reversed many aspects of immunopathology in infected MISTRG6-hACE2 mice (manuscript in revision[12]). Remdesivir and anti-IFNAR2 alone were partially therapeutic and reversed chronic weight loss and many aspects of immune-activation albeit slower than the combined therapy (Fig. 1B). Combined therapy of Remdesivir and anti-IFNAR2 however achieved rapid weight recovery and profound suppression of the immune inflammatory response as effectively as dexamethasone (Fig. 1B-H), suggesting a synergistic or additive effect of Remdesivir and anti-IFNAR2 in the chronic phase of infection. Human inflammatory macrophages were largely eliminated in the lungs of animals treated with monotherapy with Remdesivir or anti-IFNAR2 and combined therapy treated mice; this contrasted with alveolar macrophages, which following therapy were restored to a frequency similar to their status in uninfected animals (Fig. 1E, F). Anti-IFNAR2 and Remdesivir combined therapy also blocked accumulation of plasmacytoid DCs (pDCs) at 14dpi (Fig. 1G). IFNA6 transcript levels were also reduced upon Remdesivir and anti-IFNAR2 therapy in line with the reduction in pDCs, which are the primary producer of IFNα, (Fig. S1A). Overall, the reduced chronic inflammatory state attenuated T cell activation in lungs (Fig. 1H) and enhanced lung tissue recovery as measured by histopathological assessment of infected lungs (Fig. 1I).

Anti-IFNAR2 and Remdesivir treatment reverses infection induced transcriptional changes, specifically the inflammatory macrophage gene signature.

Next, we assessed the impact of anti-IFNAR2 and Remdesivir combined therapy and control dexamethasone therapy on the immunological transcriptome of infected MISTRG6-hACE2 mice by focusing on differentially regulated human genes. Both dexamethasone, anti-IFNAR2 and Remdesivir therapies reversed many aspects of the overactive immune response that were established in the chronic phase at 14dpi to their levels in uninfected animals (Fig. 2A, S2A). The reduced transcripts included chemokines and cytokines (CXCL10, CXCL8), inflammatory response (TLR7, CASP1) and anti-viral molecules (MPO, OAS1, OAS2), and ISGs (IFITM3, IFITM2, IRF7). In line with the similarities in flow cytometric assessment of immune cells and their states, dexamethasone suppressed genes significantly overlapped with genes significantly suppressed by anti-IFNAR2 and Remdesivir combined therapy (64% overlap, Fig. 2A, S2B). These genes were particularly enriched for chemokine and cytokine networks involved in hyperactivation during viral infections and ISGs (Fig. S2B-D), emphasizing the central role for IFN signaling and inflammatory cytokine chemokine networks in chronic COVID-19 pathology. To gain a deeper understanding of transcriptional changes at the cellular level we compared the single cell transcriptomes of human immune cells from infected mice late in disease with their uninfected counterparts. We identified 16 clusters that corresponded to multiple subsets of T cells, monocytes, macrophages, and B cells (Fig. 2B, S2E). To identify differentially abundant (DA) subpopulations not restricted to clusters, we applied DA-seq, a targeted, multiscale approach that quantifies a local DA measure for each cell for comprehensive and accurate comparisons of transcriptomic distributions of cells[15]. DA-seq analysis on our data revealed that T cells, monocytes and macrophages were responsible for the majority of the chronic infection driven changes (Fig. 2C). We focused our efforts on deeper characterization of monocyte/macrophage clusters at early (4dpi) or late (14 and 28dpi) infection. This analysis allowed step by step characterization of the inflammatory macrophage response during the later course of SARS-CoV-2 infection (Fig. 2D). Tissue resident macrophages such as alveolar macrophages which are the sentinels of lung infection responded at the peak of infection (Fig. 2D, S2F cluster 2,3), but the pathology and inflammatory responses were driven by infiltrating monocytes and monocyte-derived macrophages (Fig. 2D, S2F clusters 0 and 1). Although these macrophages further differentiated during the course of infection, they maintained their inflammatory signature and activated status evidenced in enriched or sustained expression of chemokines (CXCL8), inflammatory markers (TREM1) and complement involvement (C1QB) at 28dpi (Fig. S2G, H). Interestingly, all macrophage subsets throughout were enriched for ISGs at the time points assayed (Fig. S2H). These ISG enriched genes that are upregulated in macrophages at 14dpi or 28dpi were suppressed upon anti-IFNAR2 and Remdesivir

combination therapy starting at 14dpi but with a stronger effect at 28dpi (Fig. 2E). These findings together suggest that anti-IFNAR2 and Remdesivir therapy delivered in the chronic phase of infection attenuates the inflammatory macrophage response which is driven by viral RNA and sustained IFN signaling. Finally, we quantified how therapeutics impacted expression of a representative list of ISGs (DDX58, IFIH1, IFITM3, IRF7) or inflammatory markers (IL6), based on their conserved or shared expression pattern by different clusters and sustained enrichment in late disease (14dpi and 28dpi). Expression of all these representative genes was reduced in response to these therapeutics (Fig. S2I). Some of these, such as IFITM3, IL6 were particularly enriched in macrophage/monocyte clusters, while other such as IRF7, DDX58 and IFIH1 were enriched in multiple immune cells such as T cells, B cells and myeloid cells (Fig. S2I). Yet, key anti-viral responses such as IFNG production primarily mediated by cytotoxic T cells were not decreased (Fig. S2J) despite reduced T cell activation (Fig. 1H), further highlighting strong but selective effects of anti-IFNAR2 and Remdesivir therapy on chronic COVID-19 pathology in humanized mice. This reversal of immunopathology also correlated with improved lung health as measured by loss of the gene signature associated with pre-alveolar type 1 transitional cell state (PATS) in pneumocytes induced during human patient lung injury[11,16-18]. Consistent with the observed fibrosis, severe COVID-19 lungs versus healthy lungs were highly enriched for the PATS program in pneumocytes[11]. In infected MISTRG6-hACE2 mice, both dexamethasone and anti-IFNAR2 and Remdesivir combined therapy were effective in reversing this PATS program to its baseline uninfected state (Fig. S2K).

SARS-CoV-2 replicates in human macrophages.

Next, we set out to determine the cellular source of persistent viral RNA and sustained viral replication in lung, as measured by genomic and subgenomic viral RNA, respectively, in whole lung tissue (Fig. S3A). Viral RNA declined upon treatment with Remdesivir, an inhibitor of viral RNA-dependent RNA polymerase (RdRp)[13]. Moreover, Remdesivir treatment reduced viral titers and subgenomic viral RNA to undetectable levels (Fig. S3B, C). To determine the cellular source of viral RNA, we sorted epithelial cells or human immune cells from infected MISTRG6-hACE2 mice. As expected, we could detect viral RNA in epithelial cells, the main targets of SARS-CoV-2 infections. To our surprise, however, human immune cells also had similar levels of viral RNA (Fig. 3A). Although genomic RNA was abundant, we could not detect any subgenomic RNA in either sorted total epithelial cells or human immune cells, suggesting that only a fraction of the cells was infected. To better visualize and characterize these cells, we infected MISTRG6-hACE2 mice with a reporter strain of virus, SARS-CoV-2-mNG[19]. The

majority of epithelial cells (EPCAM+) in bronchioalveolar lavage (BAL) but only a small proportion of total lung epithelial cells were infected with SARS-CoV-2 as measured by mNG expressing cells (Fig. 3B). This assay was specific, as only mice infected with reporter SARS-CoV-2-mNG, but not with control wild type SARS-CoV-2/WA1, had mNG signal in their epithelial cells (Fig. 3B). Human immune cells showed a clear mNG signal, as has been suggested from measuring viral RNA levels; mNG+ human immune cells were predominantly human macrophages (Fig. 3C, S3D). In contrast, neither mouse macrophages nor mouse immune cells had significant mNG signals suggesting that only human immune cells can be infected with mNG (Fig. 3C, S3D). However, since macrophages are phagocytic, we needed to address whether the SARS-CoV-2 viral RNA in these cells replicates in these cells or is simply acquired by phagocytosis of infected cells or debris. To achieve this, we first characterized the mNG signal in human macrophages from MISTRG6 mice that were not transduced with hACE2. In these mice, epithelial cells were not infected with SARS-CoV-2 in particular due to differences between mouse and human ACE2 that limit viral entry and replication[20]. These mice had however similar levels of mNG signal in the human macrophages of AAV- ACE2 mice, arguing that viral uptake by human macrophages is independent of infected epithelial cells (Fig S3E). To determine whether SARS-CoV-2 replicates in human macrophages, we measured the key characteristics of viral replication, viral replication products, subgenomic RNA, double stranded RNA (dsRNA), and the key replicative enzyme RNA dependent RNA polymerase (RdRp). First, we quantified genomic and subgenomic viral RNA in mNG+ vs mNG- epithelial or human immune cells at 4dpi or 14dpi. Only mNG+ epithelial cells and mNG+ human immune cells but not mNG- cells had detectable subgenomic viral RNA (Fig. 3D). The levels of subgenomic RNA in human immune cells and epithelial cells were similar, suggesting a similar extent of viral replication in human immune cells and epithelial cells (Fig. 3D). Second, we stained for dsRNA in mNG+ cells to determine whether the mNG signal colocalized with dsRNA, an exclusive product of viral replication (Fig. S3F). As expected, mNG and dsRNA were detectable and colocalized in both epithelial cells and in macrophages as identified by MARCO, a marker of tissue resident macrophages (Fig. 3E, S3F, G), further corroborating viral replication in infected human macrophages. Third, we could visualize viral RdRp in human macrophages, albeit at a lower intensity than seen in infected epithelial cells (Fig. 3F, S3G). We tested whether Remdesivir, an inhibitor of RdRp could block the mNG signal. We treated (starting at 1dpi) infected MISTRG6-hACE2 mice to determine if this viral replication measured by mNG signal is inhibited. Indeed, mice treated with Remdesivir had reduced mNG signal that corresponded to similarly reduced viral titers (Fig. 3G).

SARS-CoV-2 uptake by human macrophages is enhanced by antibodies.

Antibodies can mediate viral uptake by macrophages, for example in Dengue virus infection[21]. To test the role of antibody mediated viral uptake by macrophages, we treated infected mice with monoclonal antibodies against Spike protein of SARS-CoV-2 [22], starting at 35 hours post infection (hpi). Indeed, monoclonal antibody treatment increased the percentage of mNG+ macrophages in lungs (Fig. 3H). To elucidate whether these effects are the result of bona-fide infection, or due to opsonization of infected cells which would promote phagocytosis of infected cells, we cultured bone-marrow (BM) derived macrophages with SARS-CoV-2 *in vitro* in presence or absence of patient plasma from COVID19 patients. Indeed, SARS-CoV-2 can be taken up by BM-derived macrophages and replicates in these cells as measured by mNG signal (Fig S3H) and high levels of subgenomic viral RNA (Fig S3K). This was true for different types of macrophages as BM derived macrophages (either differentiated from whole bone marrow or sorted monocytes) and lung macrophages obtained from uninfected MISTRG6 mice could all be infected to the same extent (Fig. S3I), as measured by mNG signal. Viral uptake, which was enhanced by antibodies against SARS-CoV-2, and viral replication was reduced by RdRp blockade (Remdesivir) (Fig S3J).

Discussion:

The MISTRG6 model of COVID-19 faithfully reflects many of the chronic immunoinflammatory features of the human disease and provides an opportunity to dissect the mechanisms of late immunopathogenesis in this disease[12]. As in severe human disease, COVID-19 in MISTRG6-hACE2 mice presents with persistent viral RNA, chronic IFN response accompanied with a chronic inflammatory state in macrophages, delayed antibody production and systemic lymphopenia, all of which may eventually contribute to the development of pulmonary fibrosis supported by histopathological and transcriptional analysis of lungs late in infection[12]. Overall, our mechanistic study of this model here defines a cascade of events, which, following lung epithelial infection continues around 2 days later with viral or infected cell uptake by tissue resident macrophages. SARS-CoV-2 replicates at least partially in these macrophages generating replicative intermediates and activating an inflammatory program. Viral products in macrophages include dsRNA, subgenomic viral RNA, visualization of viral RNA polymerase (RdRp) and expression of a virally encoded fluorescent reporter gene, all of which is inhibited by Remdesivir, an inhibitor of viral replication.

SARS-CoV-2 viral RNA was detected in mononuclear phagocytes characterized by scRNA-seq analysis of autopsied lungs of COVID-19 patients [11,23]. In line with our findings, $CD14^{hi}CD16^{hi}$ cells and alveolar macrophages were particularly enriched with viral RNA[11,23]., Notably, these cells did not co-express the traditional viral entry factors, ACE2 and TMPRSS2[8]. Although viral uptake and the subsequent antiviral immune response, is enhanced in presence of monoclonal antibodies in our model, the outcome of this enhancement does not appear to be pathological when given early. This is in line with extensive clinical findings that show patients given convalescent plasma or monoclonal antibodies responded well to therapy and did not present with disease enhancement[24,25].

The essential role of IFNs in the early phase of disease[26,27] is also evidenced in our model by drastically higher viral loads and precipitous decline in health when the antiviral response is disabled too early by dexamethasone treatment at the peak of infection (manuscript in revision[12]). However, while the early anti-viral immune response is crucial for disease control, this same response when persistent can be pathogenic[28]. We found that targeting either chronic viral replication or the late IFN response therapeutically *in vivo* attenuates many aspects of the overactive immune-inflammatory response, especially the inflammatory macrophage response.

Overall, combination of Remdesivir and anti-IFNAR2 antibodies could be an effective therapy for chronic COVID-19 which spares the antiviral T cell response unlike dexamethasone. More generally, the findings from our study and its implications provide alternative therapeutic avenues to be explored in the clinic and may guide novel therapeutic developments and prompt clinical trials to investigate combinatorial therapies that target viral RNA and sustained IFN response.

Acknowledgements:
The generation of the original MISTRG6 model was supported by the Bill and Melinda Gates Foundation. We thank G. Yancopoulos, D. Valenzuela, A. Murphy, and W. Auerbach at Regeneron Pharmaceuticals who generated, in collaboration with our groups, the individual knock-in alleles combined in MISTRG. We thank H. Steach, M. Chiorazzi, I. Odell, E. Eynon, and W. Philbrick and all the other members of the Flavell lab for discussions and comments; J. Alderman, C. Lieber, and E. Hughes-Picard for administrative assistance; P. Ranney, C. Hughes for mouse colony management; D. Urbanos for human CD34+ cell isolation; L. Devine and E. Manet for help with cell sorting; R. Filler for help with viral stocks and cell lines. E. Sefik

is a HHMI Fellow of the Damon Runyon Cancer Research Foundation (DRG-2316-18). This work was funded by the Howard Hughes Medical Institute (RAF, MCN, and AI)). This study was also supported in part by awards from National Institute of Health grants, R01AI157488 (AI), F30CA239444 (ES), 2T32AI007517 (BI), AI061093(EM), AI118855(EM), CA016359 (EM), K08 AI128043 (CBW), U01 CA260507 (SH), Burroughs Wellcome Fund (CBW), Patterson Foundation (CBW), Fast Grant from Emergent Ventures at the Mercatus Center (AI, CBW), Mathers Foundation (AI, CBW, EM), and the Ludwig Family Foundation (AI, CBW).

Data Availability:

All data that support the findings of this study are available within the paper and its Supplementary Information files. All 10x Genomics single cell RNA sequencing and bulk RNA sequencing data that support the findings of this study will be deposited in the Gene Expression Omnibus (GEO) repository with an accession code to be determined.

Competing financial interests

The authors declare no competing financial interests.

Figure Legends:

Figure 1.

A. Schematic of experimental design of remdesivir, anti-IFNAR2 or dexamethasone treatment. SARS-CoV-2 infected MISTRG6-hACE2 mice were treated with dexamethasone and Remdesivir on days 7,8,9 post-infection with anti-IFNAR2 at 7dpi and 11 dpi. Mice were analyzed either at 14dpi or 28dpi.
B. Weight change in treated or control mice during SARS-CoV-2 infection plotted as percent change compared with original weight prior to viral inoculation. Mice were treated with remdesivir, dexamethasone at 7,8,9 dpi, with anti-IFNAR2 at 7,11 dpi or a combination of Remdesivir and anti-IFNAR2. N=4-6. Unpaired, two-tailed t-test. Mean with SD.
C. Human immune cells in 14dpi lungs and BAL of MISTRG6-hACE2 mice treated with dexamethasone, remdesivir, anti-IFNAR2 or a combined therapy of Remdesivir and anti-IFNAR2. Mean with SD. Unpaired, two-tailed t-test.
D. Human immune cells in 28dpi lungs of MISTRG6-hACE2 mice treated with dexamethasone, Remdesivir, anti-IFNAR2 or a combined therapy of Remdesivir and anti-IFNAR2. Mean with SD. Unpaired, two-tailed t-test.
E. Human macrophages in 14dpi or 28dpi lungs of treated or untreated MISTRG6-hACE2 mice. Infected MISTRG6-hACE2 were treated with dexamethasone, remdesivir, anti-IFNAR2 or a combined therapy of Remdesivir and anti-IFNAR2.
F. Representative flow cytometry plots and frequencies of alveolar macrophages or inflammatory macrophages in 14dpi or 28dpi lungs of treated or untreated MISTRG6-hACE2 mice. Mean with SD. Unpaired, two-tailed t-test.
G. Frequencies (left) and numbers (right) of pDCs at 14dpi in the lungs of treated or control mice. N=4-6. Mean with SD. Unpaired, two-tailed t-test.

H. Representative histograms for HLA-DR expression in lung T cells and frequencies of HLA-DR+ activated T cells at 14dpi or 28dpi in treated or control mice. N=6. Unpaired, two-tailed t-test. Mean with SD. Unpaired, two-tailed t-test.
I. Representative images of H&E staining and box and whisker plot (min to max) of the histopathological scores of MISTRG6-hACE2 mice treated with a combined therapy of Remdesivir and anti-IFNAR2. N=3-6.

Figure 2.

A. Heatmap of genes that are suppressed by dexamethasone or a combined therapy of Remdesivir and anti-IFNAR2. (Log2, Foldchange >-1; P adj<0.05). Transformed normalized counts in lungs of uninfected or infected MISTRG6-hACE2 mice that are therapeutically treated or left untreated (Pearson's Correlation). Row min and max of transformed values, calculated by subtracting row mean and diving by standard deviation for each gene across all samples, are visualized.
B. t-distributed stochastic neighbor embedding (*t*-SNE) plot with clustering results of scRNA-seq of human immune cells from uninfected lungs or infected lungs at 28dpi. Single cell suspensions of sorted human lung immune cells were processed and sequenced.
C. Differentially abundant populations between uninfected and infected lung human immune cells identified by DA-seq. DA-seq is a targeted, multiscale approach that quantifies a local DA measure for each cell for comprehensive and accurate comparisons of transcriptomic distributions of cells[15].
D. t-distributed stochastic neighbor embedding (*t*-SNE) plot of human monocyte and macrophage clusters from 4dpi, 14dpi and 28dpi and uninfected lungs.
E. Heatmap of genes that were identified to be differentially regulated at 14dpi and 28dpi (Fig 3D) in monocytes and macrophages. Expression of these genes in response to the combined therapy of Remdesivir and anti-IFNAR2 is plotted.

Figure 3.

A. Viral RNA in sorted human immune cells (human CD45+) or epithelial cells (mouse Epcam+) from lungs of mice infected with SARS-CoV-2.
B. mNG signal in epithelial (Epcam+) cells from lungs and BAL of mice infected with reporter SARS-CoV-2-mNG or control wild type SARS-CoV-2/WA1. mNG is expressed in infected cells following viral replication.
C. Representative flow cytometry plots of mNG signal vs human CD68 or mouse F4/80 expression and frequencies of mNG+ cells in lung immune cells (mouse and human) from MISTRG6-hACE2 mice infected with reporter SARS-CoV-2-mNG. Unpaired, two-tailed t-test.
D. Quantification of genomic and subgenomic viral RNA (E gene) in sorted mNG+ or mNG- epithelial cells or human immune cells.
E. Representative florescent microscopy images of double stranded RNA (J2 antibody), anti-MARCO antibody and DAPI staining in fixed lung tissue at 4dpi.
F. Representative florescent microscopy images of RNA dependent RNA polymerase (RdRp), anti-CD68 antibody and DAPI staining in fixed lung tissue at 4dpi.
G. mNG+ cells within human immune cells from Remdesivir treated or control untreated MISTRG6-hACE2 mice infected with SARS-CoV-2-mNG.
H. Representative flow cytometry plots and frequencies of mNG signal in human immune cells in infected mice (4dpi) treated therapeutically with monoclonal antibodies (mAb) at 35hpi. Paired, two-tailed t-test.

Supplementary Figure Legends:

Figure S1:

A. IFNA transcript levels measured by qPCR in treated or control untreated MISTRG6-hACE2 mice infected with SARS-CoV-2.

Figure S2:

A. Similarity comparison of uninfected, infected, and therapeutically manipulated lungs based on dexamethasone suppressed genes. Pearson correlation.

B. Genes suppressed by both dexamethasone and combined therapy of Remdesivir and anti-IFNAR2 (Log2, Foldchange >-1, P adj<0.05).
C. Network analysis (STRING) of genes suppressed by both dexamethasone and combined therapy of Remdesivir and anti-IFNAR2 (as shown n in S2B).
D. Pathway (Ingenuity) analysis of genes suppressed by both dexamethasone and combined therapy of Remdesivir and anti-IFNAR2 (as shown n in S2B).
E. Cluster identifying genes comparing human immune cells from infected (28dpi) or uninfected lungs.
F. Cluster identifying genes comparing human monocytes and macrophages from infected (4, 14 or 28dpi) or uninfected lungs.
G. Temporal distribution of transcriptional changes associated with monocytes and macrophages in infected (4, 14 or 28dpi) or uninfected lungs.
H. Top: Heatmap of representative genes that are differentially regulated (DEGs) in human macrophages from 4, 14, 28dpi lungs compared with uninfected lungs. Bottom: Distribution of interferon stimulated genes within these DEGs.
I. Relative expression of interferon inducible or inflammatory genes in treated or untreated MISTRG6-hACE2 mice infected with SARS-CoV-2 mice at 14dpi or 28dpi. Uninfected baseline expression values are presented as reference. Normalized to HPRT1.
J. Relative expression of IFNG in treated or untreated MISTRG6-hACE2 mice infected with SARS-CoV-2 mice at 14dpi or 28dpi. Uninfected baseline expression values are presented as reference. Normalized to HPRT1.
K. Pre-alveolar type 1 transitional cell state (PATS) associated genes that are enriched at 14dpi DEGs compared with uninfected lungs and their response to therapeutics. PATS gene signature was shown to be enriched in autopsied lungs of patients with severe COVID-19[11].

Figure S3.

A. Quantification of genomic and subgenomic viral RNA in whole homogenized lung tissue at 4, 14 and 28dpi.
B. Quantification of genomic and subgenomic viral RNA in whole homogenized lung tissue at 14dpi in mice treated with combined therapy of Remdesivir and anti-IFNAR2.
C. Quantification of genomic and subgenomic viral RNA in whole homogenized lung tissue at 28dpi in mice treated with Remdesivir, anti-IFNAR2 or combined therapy of Remdesivir and anti-IFNAR2.
D. Representative histograms of mNG expression in human or mouse lung macrophages isolated from BAL of infected MISTRG6-hACE2 mice at 4dpi.
E. Frequencies of mNG+ cells within human macrophages (hCD68+) isolated from lungs of infected MISTRG6 mice transduced with AAV-hACE2 (+AAV) or not (-AAV). MISTRG6 mice with and without AAV-hACE2 were reconstituted with human progenitor cells from the same donor.
F. Representative fluorescent microscopy images showing colocalization of double stranded RNA (J2 antibody) staining, mNG signal and DAPI staining in fixed lung tissue at 4dpi.
G. Representative fluorescent microscopy images showing colocalization of double stranded RNA (J2 antibody), RNA dependent RNA polymerase (RdRp), mouse EpCAM and DAPI staining in fixed lung tissue at 4dpi.
H. Representative histograms and frequencies of mNG+ cells in bone marrow derived macrophages cultured (or not) with SARS-CoV-2-mNG. Cells were treated with pooled plasma from healthy controls or convalescent COVID-19 patients. mNG+ macrophages were pre-gated on live (live-dead stain negative) cells at 48hpi.

I. Representative histograms and frequencies of mNG+ cells in bone marrow derived macrophages and lung macrophages cultured with SARS-CoV-2 in presence of plasma of convalescent COVID-19 patients. mNG+ macrophages were pre-gated on live (live-dead stain negative) cells at 48hpi.
J. Representative histograms and frequencies of mNG+ cells in bone marrow derived macrophages cultured with SARS-CoV-2 in presence or absence of Remdesivir. Mean with SD, unpaired t- test.

Materials and Methods

Mice

MISTRG6 was generated by the R. Flavell laboratory by combining mice generated by this lab, the laboratory of Markus Manz and Regeneron Pharmaceuticals based on the *Rag2-/- IL2rg-/-* 129xBalb/c background supplemented with genes for human M-CSF, IL-3, SIRPα, thrombopoietin, GM-CSF and IL-6 knocked into their respective mouse loci [29,30]. MISTRG6 mice are deposited in Jackson Laboratories and made available to academic, non-profit, and governmental institutions under a Yale-Regeneron material transfer agreement (already approved and agreed to by all parties). Instructions on obtaining the material transfer agreement for this mouse strain will be available along with strain information and upon request**.** All mice were maintained under specific pathogen free conditions in our animal facilities (either Biosafety Level 1, 2 or 3) under our Animal Studies Committee-approved protocol. Unconstituted MISTRG6 mice were maintained with cycling treatment with enrofloxacin in the drinking water (Baytril, 0.27 mg/ml). All animal experimentations were performed in compliance with Yale Institutional Animal Care and Use Committee protocols. For SARS-CoV-2–infected mice, all procedures were performed in a BSL-3 facility with approval from the Yale Institutional Animal Care and Use Committee and Yale Environmental Health and Safety.

Transplantation of human CD34+ hematopoietic progenitor cells into mice.

Fetal liver samples were cut in small fragments, treated for 45 min at 37 °C with collagenase D (Roche, 200 µg/ml), and prepared into a cell suspension. Human CD34+ cells were purified by performing density gradient centrifugation (Lymphocyte Separation Medium, MP Biomedicals), followed by positive immunomagnetic selection with EasySep ™ Human CD34 Positive Selection Kit (Stemcell). For intra-hepatic engraftment, newborn 1–3-day-old pups were injected with 20,000 fetal liver CD34+ cells in 20 µl of PBS were injected into the liver with a 22-gauge needle (Hamilton Company). All use of human materials was approved by the Yale University Human Investigation Committee.

AAV-hACE2 administration

AAV9 encoding hACE2 was purchased from Vector Biolabs (AAV9-CMV-hACE2). Animals were anaesthetized using isoflurane. The rostral neck was shaved and disinfected. A 5-mm incision was made, and the trachea was visualized. Using a 32-G insulin syringe, a 50-µl injection dose of 10^{11} genomic copies per milliliter of AAV-CMV-hACE2 was injected into the trachea. The incision was closed with 4–0 Vicryl suture and/or 3M Vetbond tissue adhesive. Following administration of analgesic animals were placed in a heated cage until full recovery. Mice were then moved to BSL-3 facilities for acclimation.

SARS-CoV-2 infection

SARS-CoV-2 isolate USA-WA1/2020 was obtained from BEI reagent repository. All infection experiments were performed in a Biosafety Level 3 facility, licensed by the State of Connecticut and Yale University. Mice were anesthetized using 20% vol/vol isoflurane diluted in propylene glycol. Using a pipette, 50 µl of SARS-CoV-2 (1-3x10^6 PFU) was delivered intranasally.

Therapeutics:
SARS-CoV-2 infected MISTRG6-hACE2 were treated with dexamethasone at 10mg/kg for 3 days starting at 7dpi. Mice were treated subcutaneously with Remdesivir at 25mg/kg dosing as has been previously described[31] for 3 consecutive days starting at 7dpi. Mice were treated with anti-IFNAR2 antibody at 1.5mg/kg dosing on days 7 and 11 post infection.

Viral titers
Mice were euthanized in 100% isoflurane. Approximately half of the right lung lobe was placed in a bead homogenizer tube with 1 ml of PBS + 2% FBS. After homogenization, 300 µl of this mixture was placed in 1mL Trizol (Invitrogen) for RNA extraction and analysis. Remaining volume of lung homogenates was cleared of debris by centrifugation (3,900 g for 10 min). Infectious titers of SARS-CoV-2 were determined by plaque assay in Vero E6 (standard) or Vero ACE2+TMPRSS2+ (sensitive) cells in DMEM 4% FBS, and 0.6% Avicel RC-581[32]. Plaques were resolved at 48 h after infection by fixing in 10% formaldehyde for 1 hour followed by staining for 1 hour in 0.5% crystal violet in 20% ethanol. Plates were rinsed in water to visualize plaques. Multiple dilutions of lung homogenates were used to quantify Infectious titers (minimum number of plaques that can be quantified= 10 per ml of lung homogenate).

Viral RNA analysis
RNA was extracted with the RNeasy mini kit (Qiagen) per the manufacturer's protocol. SARS-CoV-2 RNA levels were quantified using the Luna Universal Probe Onestep RT-qPCR kit (New England Biolabs) and US CDC real-time RT-PCR primer/probe sets for 2019-nCoV_N1. For each sample, 1 ug of RNA was used. Subgenomic viral RNA was quantified using primer and probe sets targeting E gene as has been previously described[33,34]. The primer-probe sequences were as follows: E_Sarbeco_F primer: ACAGGTACGTTAATAGTTAATAGCGT (400 nM per reaction);
E_Sarbeco probe _P1: FAM-ACACTAGCCATCCTTACTGCGCTTCG-BBQ (200nM per reaction); E_Sarbeco_R primer ATATTGCAGCAGTACGCACACA (400 nM per reaction); E leader specific primer sgLead-F: CGATCTCTTGTAGATCTGTTCTC (400 nM per reaction).

Histology and Immunohistochemistry
Yale pathology kindly provided assistance with embedding, sectioning of lung tissue. A pulmonary pathologist reviewed the slides blinded and identified immune cell infiltration and other related pathologies. Paraffin embedded lung tissue sections were deparaffinized in xylene and rehydrated. After antigen retrieval with 10 mM Sodium Citrate pH 6, the slides were blocked with 5% BSA in PBS with 0.1% Tween 20 for an hour. Then the samples were incubated with primary antibodies diluted in 1%BSA overnight at 2-8 °C. The next day the samples were washed and incubated with fluorescent secondary antibodies. After washes the samples were mounted on DAPI mounting media.

Isolation of cells and flow cytometry
All mice were analyzed at approximately 9-11 weeks of age. Single cell suspensions were prepared from blood, spleen BAL and lung. Mice were euthanized with 100% isoflurane. BAL was performed using standard methods with a 22G Catheter (BD). Blood was collected either retro-orbitally or via cardiac puncture following euthanasia. BAL was performed using standard methods with a 22G Catheter (BD)[35]. Lungs were harvested, minced, and incubated in a digestion cocktail containing 1 mg/ml collagenase D (Sigma) and 30 µg/ml DNase I (Sigma-Aldrich) in RPMI at 37°C for 20 min. Tissue was then filtered through a 70-µm filter. Cells were treated with ammonium- chloride-potassium buffer and resuspended in PBS with 1% FBS. Mononuclear cells were incubated at 4C with human (BD) and mouse (BioxCell, BE0307) Fc

block for 10 min. After washing, primary antibody staining was performed at 4C for 20 min. After washing with PBS, cells were fixed using 4% paraformaldehyde. For intracellular staining, cells were washed with BD permeabilization buffer and stained in the same buffer for 45 min at room temperature. Samples were analyzed on an LSRII flow cytometer (BDBiosciences). Data were analyzed using FlowJo software.

In vitro infection with SARS-CoV-2

Using aseptic techniques under sterile conditions, bone marrow cells were isolated from femurs of reconstituted MISTRG6 mice. For differentiation into macrophages, bone marrow cells were incubated in media supplemented with 10% FBS, 1% penicillin/streptomycin and recombinant human M-CSF (50ng/ml), GM-CSF (50ng/ml) and IL-4(20ng/ml) at 2x10^6 per ml concentration for 6 days in 5% CO2 incubator at 37°C. Media supplemented with 10% FBS was replenished with new media every 3–4 days. Prior to infection, cells were monitored for granularity, elongated morphology, and stronger adherence to the plate. Human macrophages were then cultured with SARS-CoV-2 in presence or absence of patient plasma and Remdesivir. To enrich for human macrophages and monocytes lung cells from uninfected MISTRG6 mice were sorted based on CD11b and human CD45 expression. These cells were then incubated with GM-CSF and IL-4 for 48 hours prior to culture with SARS-CoV-2 in presence of patient plasma.

Antibodies

Antibodies against the following antigens were used:
Mouse antigens: CD45 (Clone: 30-F11), F4/80(BM8), CD326 (G8.8); Human antigens: CD45 (HI30), CD3 (UCHT1), CD14 (HCD14), CD16 (3G8), CD19 (HIB19), CD206 (15-2), CD86 (BU63), CD68(Y1/82A), CD11B (M1/70), CD11C (3.9), HLA-DR(LN3), NKp46 (9E2), CD56(MEM-188), CD4(OKT4), CD8(SK1). All antibodies were obtained from Biolegend, unless otherwise specified. Monoclonal antibodies (clone 135 and 144) were acquired from M. Nussenzweig as has been previously described[22]. Anti-IFNAR2 antibody was purchased from PBL Assay science (Cat #21385-1). Anti-dsRNA antibody (J2) was purchased from Sigma. SARS-CoV-2 RNA-dependent RNA Polymerase Antibody was purchased from CellSignaling.

Bulk whole tissue lung RNA-sequencing

RNA isolated from homogenized lung tissue used for viral RNA analysis was also used for whole tissue transcriptome analysis. Libraries were made with the help of the Yale Center for Genomic Analysis. Briefly, libraries were prepared with an Illumina rRNA depletion kit and sequenced on a NovaSeq. Raw sequencing reads were aligned to the human-mouse combined genome with STAR[36]], annotated and counted with HTSeq[37], normalized using DESeq2[38] and graphed using the Broad Institute Morpheus web tool. Differential expression analysis was also performed with DESeq2. For IFN-stimulated gene identification, http://www.interferome.org was used with parameters -*In Vivo*, -Mus musculus or Homo sapiens -fold change up 2 and down 2.

Gene expression:

RNA was extracted with the RNeasy mini kit (Qiagen) per the manufacturer's protocol High-Capacity cDNA Reverse Transcription Kit was used to make cDNA. Quantitative reverse transcription PCR (qRT-PCR) was performed using an SYBR FAST universal qPCR kit (KAPA Biosystems). Predesigned KiCqStart primers for DDX58, IL-6, IFITM3, IRF7, IFIH1, IFNA6, IFNG and HPRT1 were purchased from Sigma.

Single Cell RNA Sequencing 10X Genomics

Single cell suspensions from digested lungs were processed for droplet based scRNA-seq and 10000 cells were encapsulated into droplets using 10X Chromium GEM technology. Libraries were prepared in house using Chromium Next GEM Single Cell 3 Reagent Kits v3.1 (10X

Genomics). scRNA-seq libraries were sequenced using Nova-Seq. Raw sequencing reads were processed with Cell Ranger 3.1.0 using a human-mouse combined reference to generate a gene-cell count matrix. To distinguish human and mouse cells, we counted the number of human genes (nHuman) and mouse genes (nMouse) with nonzero expression in each cell, and selected cells with nHuman > 20 * nMouse as human cells. The count matrix of human cells and human genes was used in the downstream analysis with Seurat 3.2[39]. Specifically, this matrix was filtered to remove low quality cells, retaining cells with > 200 and < 5,000 detected genes and < 20% mitochondrial transcripts. We then log normalized each entry of the matrix by computing log (CPM/100 + 1), where CPM stands for counts per million. To visualize the cell subpopulations in two dimensions, we applied principal component analysis followed by t-SNE, a nonlinear dimensionality reduction method, to the log-transformed data. Graph-based clustering was then used to generate clusters that were overlaid on the t-SNE coordinates to investigate cell subpopulations. Marker genes for each cluster of cells were identified using the Wilcoxon test with Seurat. For the adjusted P values the Bonferroni correction was used.
To combine cells from different DPIs, we applied the integration method[39] in Seurat to remove batch effects. We then performed principal component analysis and retained top 30 PCs as the input to tSNE, a nonlinear dimensionality reduction method, to embed the data onto 2-dimensional space for visualization. Graph-based clustering with a resolution of 0.8 was then used to generate clusters that were overlaid on the t-SNE coordinates to investigate cell subpopulations. Marker genes for each cluster of cells were identified using the Wilcoxon test with Seurat (For the adjusted P values the Bonferroni correction was used). After cell type identification, we separated out macrophage populations from all DPIs, and applied the same procedures as described above to re-preprocess and visualize the data. Clusters were redefined based on a resolution of 0.3.

Statistical Analysis

Unpaired or paired t-test was used to determine statical significance for changes in immune cell frequencies and numbers while comparing infected mice to uninfected control mice or treated mice to untreated mice. For experiments where mice were treated with therapeutics one-way ANOVA was used to determine statistical significance across groups and adjusted p value was reported. To determine whether the viral RNA quantification is statistically significant across treatment groups or time points, Mann-Whitney, two-tailed test was used. A one-sample Wilcoxon signed rank test was used to determine whether the viral titer quantification of the untreated condition is significantly different from an undetectable viral load (i.e., viral titer = 0).

References:

1 Havervall, S. *et al.* Symptoms and Functional Impairment Assessed 8 Months After Mild COVID-19 Among Health Care Workers. *JAMA* **325**, 2015-2016, doi:10.1001/jama.2021.5612 (2021).

2 Nasserie, T., Hittle, M. & Goodman, S. N. Assessment of the Frequency and Variety of Persistent Symptoms Among Patients With COVID-19: A Systematic Review. *JAMA Netw Open* **4**, e2111417, doi:10.1001/jamanetworkopen.2021.11417 (2021).

3 Gaebler, C. *et al.* Evolution of antibody immunity to SARS-CoV-2. *Nature* **591**, 639-644, doi:10.1038/s41586-021-03207-w (2021).

4 Acharya, D., Liu, G. & Gack, M. U. Dysregulation of type I interferon responses in COVID-19. *Nature Reviews Immunology* **20**, 397-398 (2020).

5 Channappanavar, R. *et al.* Dysregulated type I interferon and inflammatory monocyte-macrophage responses cause lethal pneumonia in SARS-CoV-infected mice. *Cell host & microbe* **19**, 181-193 (2016).

6 Pairo-Castineira, E. *et al.* Genetic mechanisms of critical illness in Covid-19. *Nature*, 1-1 (2020).

7 Nienhold, R. *et al.* Two distinct immunopathological profiles in autopsy lungs of COVID-19. *Nature communications* **11**, 1-13 (2020).

8 Zhou, Z. *et al.* Heightened Innate Immune Responses in the Respiratory Tract of COVID-19 Patients. **27**, 883-890 e882, doi:10.1016/j.chom.2020.04.017 (2020).

9 Dolan, M. E. *et al.* Investigation of COVID-19 comorbidities reveals genes and pathways coincident with the SARS-CoV-2 viral disease. *Scientific reports* **10**, 1-11 (2020).

10 Menter, T. *et al.* Postmortem examination of COVID-19 patients reveals diffuse alveolar damage with severe capillary congestion and variegated findings in lungs and other organs suggesting vascular dysfunction. *Histopathology* **77**, 198-209 (2020).

11 Delorey, T. M. *et al.* COVID-19 tissue atlases reveal SARS-CoV-2 pathology and cellular targets. *Nature* **595**, 107-113, doi:10.1038/s41586-021-03570-8 (2021).

12 Sefik, E. *et al.* A humanized mouse model of chronic COVID-19 to evaluate disease mechanisms and treatment options. *preprint*, doi:10.21203/rs.3.rs-279341/v1 (2021).

13 Yin, W. *et al.* Structural basis for inhibition of the RNA-dependent RNA polymerase from SARS-CoV-2 by remdesivir. *Science* **368**, 1499-1504, doi:10.1126/science.abc1560 (2020).

14 Group, R. C. Dexamethasone in hospitalized patients with Covid-19—preliminary report. *New England Journal of Medicine* (2020).

15 Zhao, J. *et al.* Detection of differentially abundant cell subpopulations in scRNA-seq data. *Proc Natl Acad Sci U S A* **118**, doi:10.1073/pnas.2100293118 (2021).

16 Strunz, M. *et al.* Alveolar regeneration through a Krt8+ transitional stem cell state that persists in human lung fibrosis. *Nat Commun* **11**, 3559, doi:10.1038/s41467-020-17358-3 (2020).

17 Kobayashi, Y. *et al.* Persistence of a regeneration-associated, transitional alveolar epithelial cell state in pulmonary fibrosis. *Nat Cell Biol* **22**, 934-946, doi:10.1038/s41556-020-0542-8 (2020).

18 Choi, J. *et al.* Inflammatory Signals Induce AT2 Cell-Derived Damage-Associated Transient Progenitors that Mediate Alveolar Regeneration. *Cell Stem Cell* **27**, 366-382 e367, doi:10.1016/j.stem.2020.06.020 (2020).

19 Xie, X. *et al.* An Infectious cDNA Clone of SARS-CoV-2. *Cell Host Microbe* **27**, 841-848 e843, doi:10.1016/j.chom.2020.04.004 (2020).

20 Li, W. *et al.* Efficient replication of severe acute respiratory syndrome coronavirus in mouse cells is limited by murine angiotensin-converting enzyme 2. *J Virol* **78**, 11429-11433, doi:10.1128/JVI.78.20.11429-11433.2004 (2004).

21 Bournazos, S., Gupta, A. & Ravetch, J. V. The role of IgG Fc receptors in antibody-dependent enhancement. *Nat Rev Immunol* **20**, 633-643, doi:10.1038/s41577-020-00410-0 (2020).

22 Davide, F. R. *et al.* Convergent Antibody Responses to SARS-CoV-2 in Convalescent Individuals. *Nature*.

23 Grant, R. A. *et al.* Circuits between infected macrophages and T cells in SARS-CoV-2 pneumonia. *Nature*, 1-10.

24 Taylor, P. C. *et al.* Neutralizing monoclonal antibodies for treatment of COVID-19. *Nat Rev Immunol* **21**, 382-393, doi:10.1038/s41577-021-00542-x (2021).

25 Bournazos, S. & Ravetch, J. V. Fcγ receptor function and the design of vaccination strategies. *Immunity* **47**, 224-233 (2017).

26 Bastard, P. *et al.* Autoantibodies against type I IFNs in patients with life-threatening COVID-19. *Science* **370**, doi:10.1126/science.abd4585 (2020).

27 Zhang, Q. *et al.* Inborn errors of type I IFN immunity in patients with life-threatening COVID-19. *Science* **370**, doi:10.1126/science.abd4570 (2020).

28 Major, J. *et al.* Type I and III interferons disrupt lung epithelial repair during recovery from viral infection. *Science* **369**, 712-717, doi:10.1126/science.abc2061 (2020).

29 Yu, H. *et al.* A novel humanized mouse model with significant improvement of class-switched, antigen-specific antibody production. *Blood* **129**, 959-969, doi:10.1182/blood-2016-04-709584 (2017).

30 Rongvaux, A. *et al.* Development and function of human innate immune cells in a humanized mouse model. *Nature Biotechnology* **32**, 364-372, doi:10.1038/nbt.2858 (2014).

31 Pruijssers, A. J. *et al.* Remdesivir Inhibits SARS-CoV-2 in Human Lung Cells and Chimeric SARS-CoV Expressing the SARS-CoV-2 RNA Polymerase in Mice. *Cell Rep* **32**, 107940, doi:10.1016/j.celrep.2020.107940 (2020).

32 Wei, J. *et al.* Genome-wide CRISPR screens reveal host factors critical for SARS-CoV-2 infection. *Cell* (2020).

33 Wolfel, R. *et al.* Virological assessment of hospitalized patients with COVID-2019. *Nature* **581**, 465-469, doi:10.1038/s41586-020-2196-x (2020).

34 Corman, V. M. *et al.* Detection of 2019 novel coronavirus (2019-nCoV) by real-time RT-PCR. *Euro Surveill* **25**, doi:10.2807/1560-7917.ES.2020.25.3.2000045 (2020).

35 Sun, F., Xiao, G. & Qu, Z. Murine bronchoalveolar lavage. *Bio-protocol* **7**, e2287 (2017).

36 Dobin, A. *et al.* STAR: ultrafast universal RNA-seq aligner. *Bioinformatics* **29**, 15-21, doi:10.1093/bioinformatics/bts635 (2013).

37 Anders, S., Pyl, P. T. & Huber, W. HTSeq--a Python framework to work with high-throughput sequencing data. *Bioinformatics* **31**, 166-169, doi:10.1093/bioinformatics/btu638 (2015).

38 Love, M. I., Huber, W. & Anders, S. Moderated estimation of fold change and dispersion for RNA-seq data with DESeq2. *Genome Biol* **15**, 550, doi:10.1186/s13059-014-0550-8 (2014).

39 Stuart, T. *et al.* Comprehensive integration of single-cell data. *Cell* **177**, 1888-1902. e1821 (2019).

Figure 1.

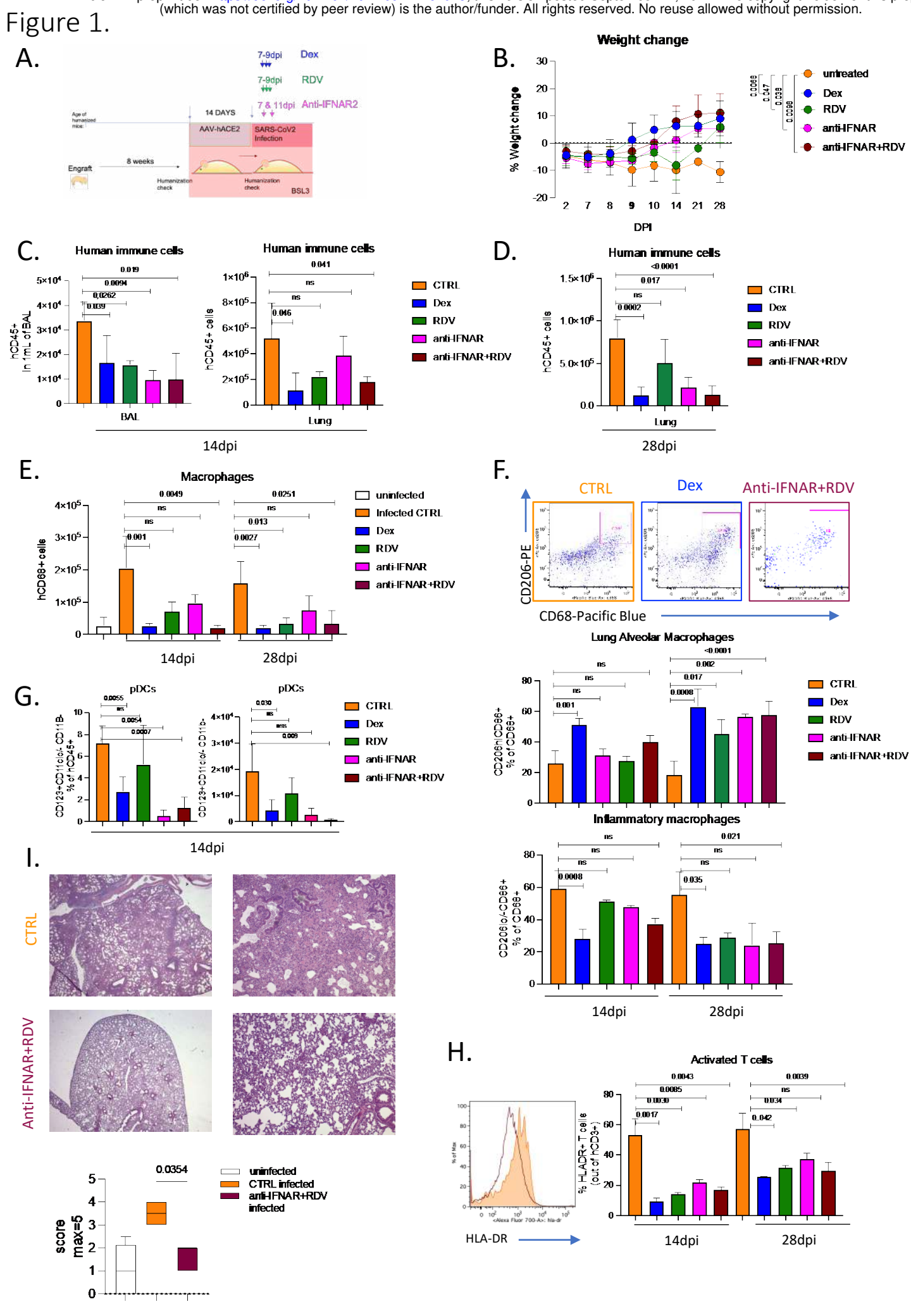

Figure 2.

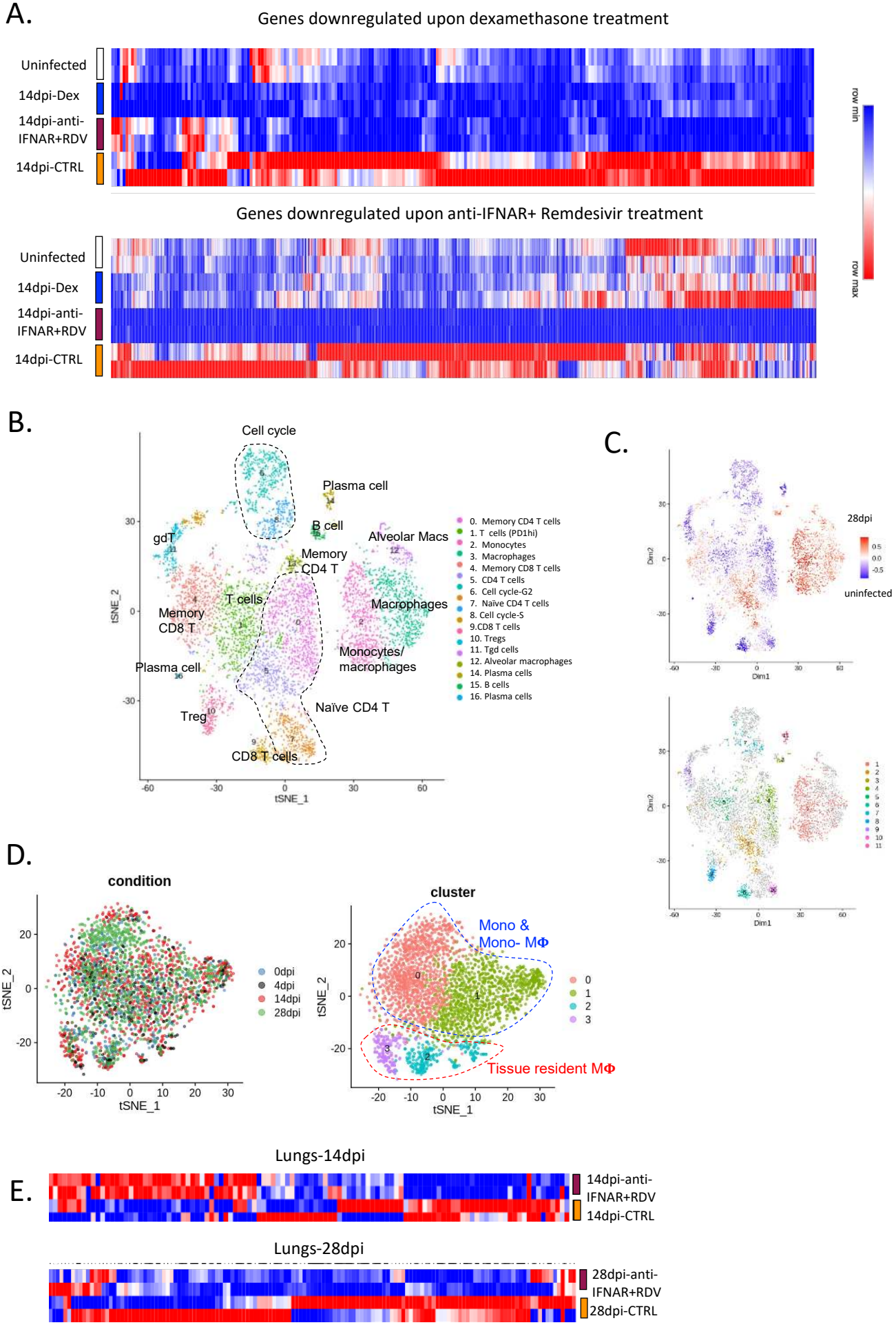

Figure 3